PCCP

ROYAL SOCIETY OF CHEMISTRY

PAPER

View Article Online
View Journal | View Issue

Cite this: *Phys. Chem. Chem. Phys.*, 2023, **25**, 17450

Colossal room-temperature electrocaloric strength aided by hydrostatic pressure in lead-free multiferroic solid solutions

César Menéndez,[a] Riccardo Rurali[b] and Claudio Cazorla *[c]

Received 22nd May 2023,
Accepted 9th June 2023

DOI: 10.1039/d3cp02318d

rsc.li/pccp

Solid-state cooling applications based on electrocaloric (EC) effects are particularly promising from a technological point of view due to their downsize scalability and natural implementation in circuitry. However, EC effects typically involve materials that contain toxic substances and require relatively large electric fields (∼100–1000 kV cm^{-1}) that cause fateful leakage current and dielectric loss problems. Here, we propose a possible solution to these practical issues that consists of concertedly applying hydrostatic pressure and electric fields on lead-free multiferroic materials. We theoretically demonstrate this strategy by performing first-principles simulations on supertetragonal $BiFe_{1-x}Co_xO_3$ solid solutions (BFCO). It is shown that hydrostatic pressure, besides adjusting the occurrence of EC effects to near room temperature, can reduce enormously the intensity of driving electric fields. For pressurized BFCO, we estimate a colossal room-temperature EC strength, defined as the ratio of the adiabatic EC temperature change by an applied electric field, of ∼1 K cm kV^{-1}, a value that is several orders of magnitude larger than those routinely measured in uncompressed ferroelectrics.

One of the limiting factors of modern microelectronic devices is their tremendous heat dissipation density, which needs to be mitigated through cooling in order to ensure appropriate performance. Current refrigeration technologies, however, rely on compression cycles of environmentally harmful gases and cannot be scaled down to microchip dimensions. Electrocaloric (EC) cooling is a highly promising solid-state refrigeration technology for the thermal management of chips and microcircuitry owing to its high efficiency, environmental friendliness, and easy miniaturization.[1] EC refrigeration exploits the reversible thermal change of ferroelectric materials resulting from phase transitions induced by external electric field variations. A large EC isothermal entropy change, ΔS_{EC}, of ∼10 J K^{-1} kg^{-1} and an adiabatic temperature change, ΔT_{EC}, of ∼1–10 K have been measured in ferroelectric materials like $BaTiO_3$,[2,3] $Pb(Zr,Ti)O_3$[4] and HfO_2,[5] to cite few examples.

Nonetheless, unfortunately, the largest EC effects observed to date normally involve materials that contain toxic substances like lead and require large electric fields that are energetically costly and produce adverse leakage currents and dielectric losses.[6–8] Recently, several materials design strategies have been proposed to overcome these common EC problems. For instance, by exploiting electrostatic coupling and interface effects in lead-free ferroelectric relaxor heterostructures, an unprecedentedly large EC adiabatic temperature shift of ≈23 K has been realized near room temperature for moderate electric bias ($\mathcal{E}_c$ ∼ 100 kV cm^{-1}).[9] Nevertheless, the magnitude of such EC effects can be strongly influenced by the specific details of the heterostructure synthesis process and thus in practice ΔT_{EC} may strongly fluctuate from one sample to another. Another recent EC advancement has been reported for the layered hybrid perovskite ferroelectric $[(CH_3)_2CHCH_2NH_3]_2PbCl_4$,[10] in which a sharp first-order ferroelectric phase transition associated with a high-entropy change occurs instead of the continuous phase transformation associated with a low-entropy change that is characteristic of inorganic ferroelectric perovskites.[11] In this case, a giant ΔT_{EC} of 11.1 K has been measured at room temperature for a small electric field of 29.7 kV cm^{-1}. However, the implicated material still contains lead and the degree of reversibility associated with such giant EC effects appears to be quite limited.

In this work, we propose a completely different approach for the enhancement of EC effects that consists of the application of multiple external fields on lead-free multiferroic materials able to undergo sharp first-order phase transitions. (Previous experimental and theoretical studies have already explored a similar approach although considering lead-containing materials and/or non-abrupt phase transitions.[12–18]) In particular, we demonstrate by means of computational first-principles methods that

[a] *School of Chemistry, The University of Sydney, NSW 2006, Australia*
[b] *Institut de Ciència de Materials de Barcelona, ICMAB–CSIC, Campus UAB, 08193 Bellaterra, Spain*
[c] *Departament de Física, Universitat Politècnica de Catalunya, 08034 Barcelona, Spain. E-mail: claudio.cazorla@upc.edu*

the sequential operation of hydrostatic pressure and electric fields in $BiFe_{1-x}Co_xO_3$ solid solutions (BFCO) can trigger large and inverse EC effects of $\Delta S_{EC} \approx 5$ J K^{-1} kg^{-1} and $\Delta T_{EC} \approx -5$ K at room temperature. Moreover, aided by pressure BFCO displays a colossal EC strength of $\sim$1 K cm kV^{-1}, defined as $|\Delta T_{EC}|/\mathcal{E}_c$,[19] which surpasses by several orders of magnitude the typical values reported for uncompressed ferroelectrics.

Results

Phase competition in BFCO under pressure

At room temperature and zero pressure, $BiFe_{1-x}Co_xO_3$ solid solutions (BFCO) can be stabilized in two different polymorphs, depending on the relative content of Fe/Co atoms, exhibiting rhombohedral ($\mathcal{R}$) and tetragonal ($\mathcal{T}$) symmetries.[20–22] For relative cobalt contents of $0 \leq x \lessapprox 0.25$, the BFCO ground state is the $\mathcal{R}$ phase, which is analogous to the ground state of bulk $BiFeO_3$.[20–23] This rhombohedral phase presents an electric polarization of 60–80 μC cm^{-2} that is oriented along the pseudocubic direction [111] (Fig. 1a) and G-type antiferromagnetic spin ordering (AFM-G, the net magnetic moment of each transition metal ion is antiparallel to those of its six first nearest neighbours). For larger relative cobalt contents, $0.25 < x$, the BFCO ground state corresponds to the $\mathcal{T}$ phase, which is analogous to the ground state of bulk $BiCoO_3$.[20–22,24,25] According to theoretical calculations, this tetragonal phase presents a giant electric polarization of 160–180 μC cm^{-2} oriented along the pseudocubic direction [001] (Fig. 1a),[20–22] and hence sometimes it is referred to as "supertetragonal", and C-type antiferromagnetic spin ordering (AFM-C, the net magnetic moment of each transition metal ion is parallel to those of its two first nearest neighbours located along the polar axis and antiparallel to those of its other four first nearest neighbours).

Under increasing temperature and for relative cobalt contents of $x \lessapprox 0.25$, the supertetragonal $\mathcal{T}$ phase can be stabilized over the $\mathcal{R}$ phase owing to its larger vibrational entropy.[20–22] Such a T-induced phase transition is clearly of first-order type (or discontinuous) since the volume change associated with it is huge ($\sim$10%). Barocaloric effects are driven by hydrostatic compression; however, to the best of our knowledge, there are no experimental studies on BFCO under pressure. Here, we amend for such a lack of information by carrying out accurate first-principles calculations based on density functional theory (DFT, Methods).[22,26] Fig. 1b shows the estimated hydrostatic pressure that is necessary to drive the $\mathcal{T} \rightarrow \mathcal{R}$ phase transition at low temperatures (*i.e.*, disregarding entropy and also likely quantum nuclear effects, which tend to slightly overestimate p_t) and for compositions in the interval $0.25 \leq x \leq 0.50$. This transition pressure is found to steadily, and significantly, decrease upon increasing Fe content. For instance, p_t amounts to 1.4 GPa at $x = 0.50$ and 0.3 GPa at $x = 0.25$. As expected, the closer the cobalt content is to the $\mathcal{T}$–$\mathcal{R}$ morphotropic phase boundary ($x_c \approx 0.25$), the easier results to switch from the supertetragonal phase to the rhombohedral phase with pressure.

Simulating temperature effects in materials using first-principles methods is computationally very intensive and laborious. However, temperature effects are critical for the assessment of possible caloric phenomena and consequently cannot be neglected in the present study. We employed the quasi-harmonic approximation (QHA)[22,26] to calculate *ab initio* Gibbs free energies for BFCO in the $\mathcal{T}$ and $\mathcal{R}$ phases under broad pressure, temperature and electric field conditions, thus allowing for the estimation of barocaloric and electrocaloric effects associated with first-order phase transitions (Methods).

Fig. 1c shows the p–T phase diagram calculated for BFCO at a composition of $x = 0.50$, hereafter referred to as $BFCO_{0.5}$. Therein, it is appreciated that p_t consistently increases upon increasing temperature, reaching a value of 1.24 GPa at room temperature. In spite of such a relatively large pressure, in what follows we present the multicaloric results obtained for bulk

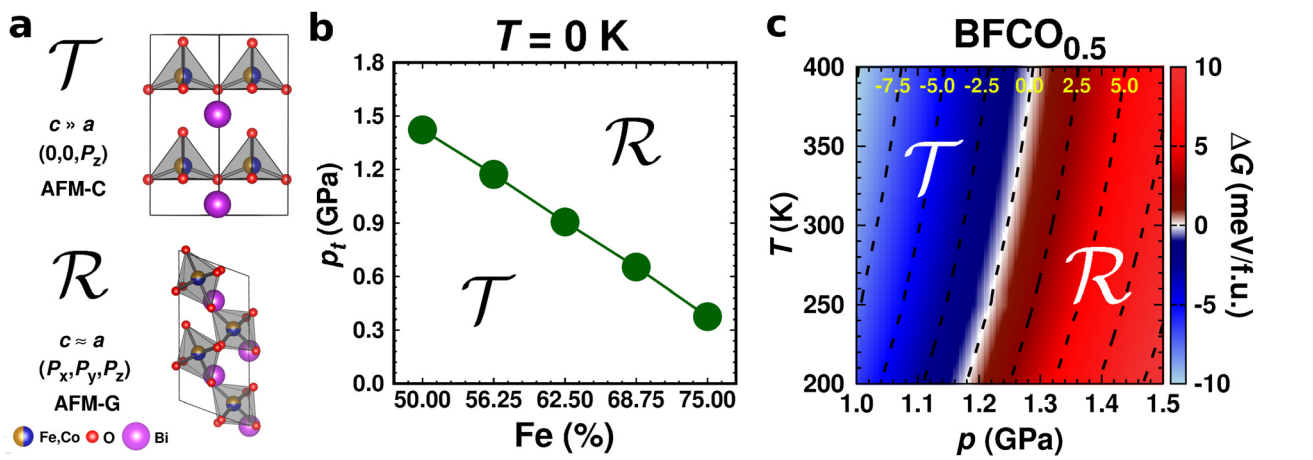

Fig. 1 Phase competition in BFCO under pressure. (a) Sketch of the competitive tetragonal ($\mathcal{T}$) and rhombohedral ($\mathcal{R}$) multiferroic phases. The corresponding electric polarization and antiferromagnetic spin ordering are indicated. (b) The $\mathcal{T} \rightarrow \mathcal{R}$ transition pressure calculated at $T = 0$ K disregarding likely quantum nuclear effects (which slightly overestimates p_t) and expressed as a function of composition. (c) First-principles p–T phase diagram of $BFCO_{0.5}$. Phase transition points were determined under the condition $\Delta G(p, T_t) \equiv G_{\mathcal{T}}(p, T_t) - G_{\mathcal{R}}(p, T_t) = 0$.

$BFCO_{0.5}$ at and near room temperature since from a computational point of view this solid solution is highly affordable (*i.e.*, the size of the corresponding simulation cells is among the smallest thus making the QHA free energy calculations feasible). In practice, much smaller pressures of the order of several 0.1 GPa can be attained by reducing the relative content of Co ions (Fig. 1b) without probably affecting the main conclusions presented in the next section (see the Discussion section).

Barocaloric performance of $BFCO_{0.5}$

We start by analyzing the barocaloric effects induced by hydrostatic pressure in bulk $BFCO_{0.5}$ in the absence of electric fields. Fig. 2a and b show the compression required to induce the $\mathcal{T} \rightarrow \mathcal{R}$ phase transition as a function of temperature, p_t, and the accompanying relative volume change. The estimated phase transition volume change is negative and very large as it amounts to $\sim$8% in absolute value. Such a huge relative volume change augurs a large phase transition entropy change, as it can be inferred from the Clausius–Clapeyron (CC) relationship $\Delta S_t = \Delta V \cdot \frac{dp_t}{dT}$. However, after performing the calculations and assuming that $\Delta S_{BC} \approx \Delta S_t$ (Methods), it was found that the ensuing barocaloric isothermal entropy shifts were actually quite modest (Fig. 2c). For instance, at room temperature, we obtained $|\Delta S_{BC}|$ = 1.7 J K^{-1} mol^{-1} (5.4 J K^{-1} kg^{-1}), which is about one order of magnitude smaller than the giant barocaloric entropy changes found in superionic and plastic crystals ($\sim$100 J K^{-1} kg^{-1}).[27–35] Under decreasing temperature, $|\Delta S_{BC}|$ slightly increases (*e.g.*, 2.8 J K^{-1} mol^{-1} at T = 200 K); however, the estimated values still are quite reduced. The reason for these outcomes is that p_t barely changes with temperature in the explored thermodynamic range (*i.e.*, the temperature derivative of the phase transition pressure amounts only to $\sim 10^{-3}$ GPa K^{-1}, Fig. 2a).

The revealed minute T-induced p_t variation, on the other hand, implies sizeable changes in the phase transition temperature, T_t, as induced by small pressure shifts (since dT_t/dp =

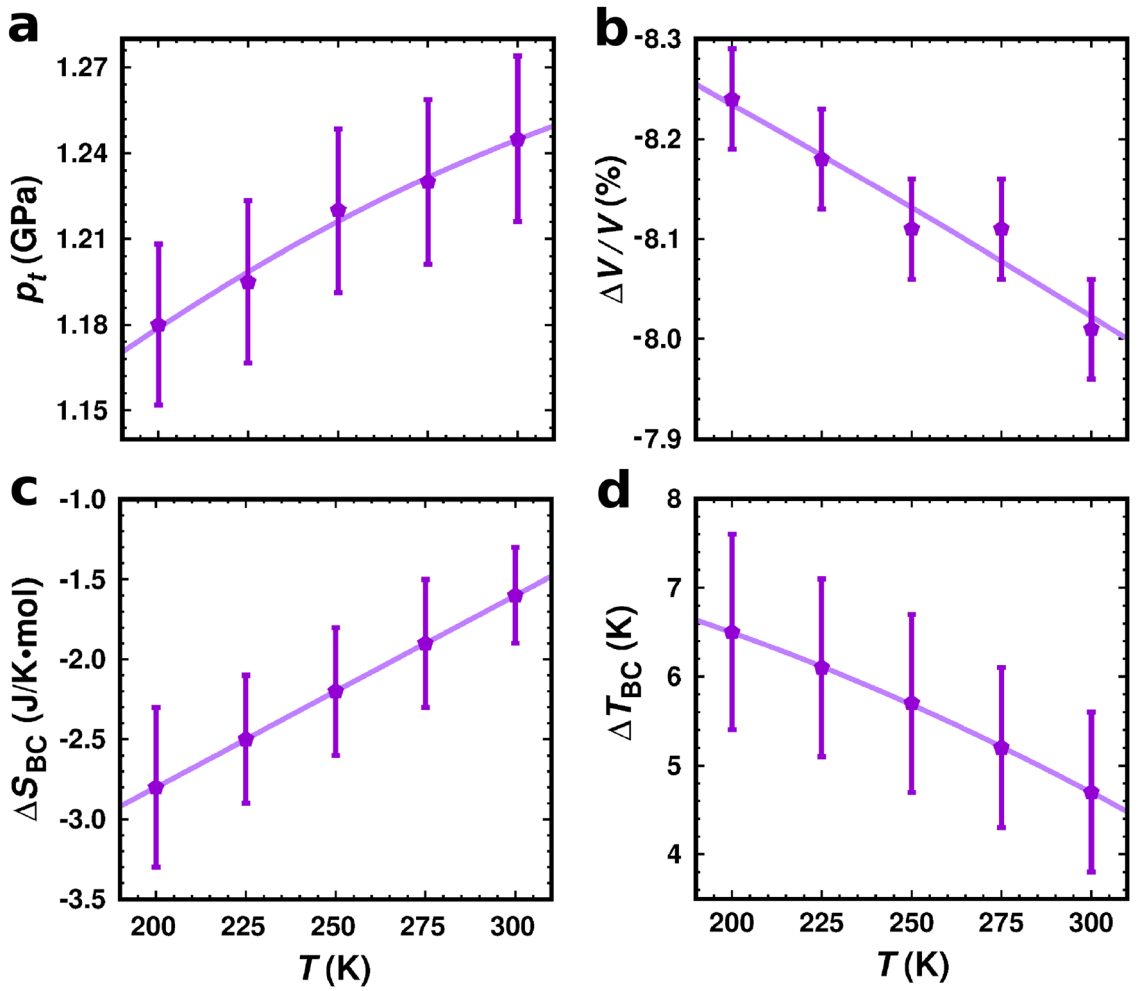

Fig. 2 Barocaloric descriptors of $BFCO_{0.5}$ estimated with DFT-based first-principles methods. (a) $\mathcal{T} \rightarrow \mathcal{R}$ phase transition pressure expressed as a function of temperature. (b) Relative volume change associated with the p-induced $\mathcal{T} \rightarrow \mathcal{R}$ phase transition as referred to the tetragonal phase. (c) Barocaloric isothermal entropy change, ΔS_{BC}, expressed as a function of temperature. (d) Barocaloric adiabatic temperature change, ΔT_{BC}, expressed as a function of temperature. Both ΔS_{BC} and ΔT_{BC} were estimated by using the Clausius–Clapeyron relationship (Methods). Solid lines in the figure are simple eye-guides.

$[dp_t/dT]^{-1}$), thus suggesting possibly large barocaloric thermal shifts in bulk $BFCO_{0.5}$. Fig. 2d shows the barocaloric adiabatic temperature changes, ΔT_{BC}, estimated as a function of temperature (Methods). At room temperature (T = 200 K), ΔT_{BC} was found to amount to 4.7 K (6.5 K) which, although it cannot rival with the barocaloric adiabatic temperature changes reported for superionic and plastic crystals ($\sim$10 K),[27–35] it shows promise in the context of electrocaloric effects ($\sim$1–10 K).

The barocaloric results presented above were obtained using the Clausius–Clayperon (CC) method, which is not exact.[27] Aimed to assess the extent of the employed approximations, we mimicked with theory quasi-direct barocaloric experiments[27,31] where entropy curves are estimated as a function of pressure and temperature and from which ΔS_{BC} and ΔT_{BC} can be straightforwardly determined (Fig. 3a and b).[35] Moreover, using this quasi-direct estimation approach it is also possible to determine, for a given pressure shift, Δp, the temperature span, T_{span}, over which barocaloric effects can be operated (Fig. 3b). In view of the huge dT_t/dp of $\sim 10^3$ K GPa^{-1} estimated for $BFCO_{0.5}$, giant T_{span} values are anticipated.[36]

Fig. 3c shows the results of our quasi-direct barocaloric descriptor estimations. At room temperature and T = 200 K, we obtained adiabatic temperature changes of 2.0 $\pm$ 2.5 and 4.0 $\pm$ 2.5 K, respectively. Within the numerical uncertainties, these results are compatible with our previous estimations obtained using the CC method; however, it goes without saying that the reported error bars are unacceptably too large. The reasons for the relatively huge numerical uncertainties on ΔT_{BC} are the small ΔS_t and great p-induced T_t shifts involved in the quasi-direct estimation (Fig. 3a). Thus, unfortunately, in the present case, it is not possible to discern the actual precision of the barocaloric adiabatic temperature changes obtained using the approximate CC method. Nevertheless, the estimation of T_{span} is still possible given its noticeably large size (Fig. 3a and b). By considering an outset compression of 1.18 GPa, we obtained a T_{span} of $\approx$ 60 K for a small pressure shift of 0.06 GPa (calculated by adding up all the ΔT_{span} increments shown in Fig. 3c). This result is very encouraging since it indicates that, in spite of the relative smallness of ΔS_{BC} and ΔT_{BC}, barocaloric effects in $BFCO_{0.5}$ could be operated over unusually ample temperature ranges.

Electrocaloric performance of pressurized $BFCO_{0.5}$

The electric polarization, P, of $BFCO_{0.5}$ in the $\mathcal{R}$ and $\mathcal{T}$ phases is significantly different; for instance, P in the supertetragonal phase is more than two times larger than that in the rhombohedral phase,[22] adding up to polarization module differences of $>$100 μC cm^{-2} (Fig. 4b). Such a huge electric polarization disparity seems very promising from an electrocaloric (EC) point of view, as it can be inferred from the electric Clausius–Clapeyron relationship $\Delta S_t = \Delta \boldsymbol{P} \cdot \frac{d\mathcal{E}_c}{dT}$, where ΔS_t represents the entropy change associated with the field-induced phase transition and $\mathcal{E}_c$ is the necessary electric field to switch from the $\mathcal{R}$ phase to the $\mathcal{T}$ phase. Fig. 4a shows the $\mathcal{E}_c$ estimated for a fixed pressure of 1.25 GPa as a function of temperature (Methods), which has been selected to ensure appropriate stabilization of the $\mathcal{R}$ phase under conditions $T \leq$ 300 K. As clearly appreciated therein, the critical electric field steadily decreases upon increasing temperature, ranging from 43 kV cm^{-1} at 200 K to $\approx$2 kV cm^{-1} at room temperature.

Fig. 4c–e show the electrocaloric isothermal entropy and adiabatic temperature changes, ΔS_{EC} and ΔT_{EC}, estimated for compressed $BFCO_{0.5}$ using the CC approach (Methods). In this case, the sign of the EC descriptors indicates that the caloric effect is inverse, that is, $\Delta T_{EC} < 0$. This result follows from the fact that the high-entropy phase $\mathcal{T}$ presenting the largest electric polarization is stabilized *via* the application of the external electric bias, namely, $\Delta S_{EC} > 0$ (conversely, in customary direct electrocaloric effects, the ferroelectric phase that is stabilized through the electric field corresponds to the low-entropy phase, thus $\Delta S_{EC} < 0$ and consequently $\Delta T_{EC} > 0$). As expected, the size and temperature dependence of $|\Delta S_{EC}|$ and $|\Delta T_{EC}|$, which are directly related among them through the temperature and heat capacity (Fig. 4d, Methods), are very much similar to those of $|\Delta S_{BC}|$ and

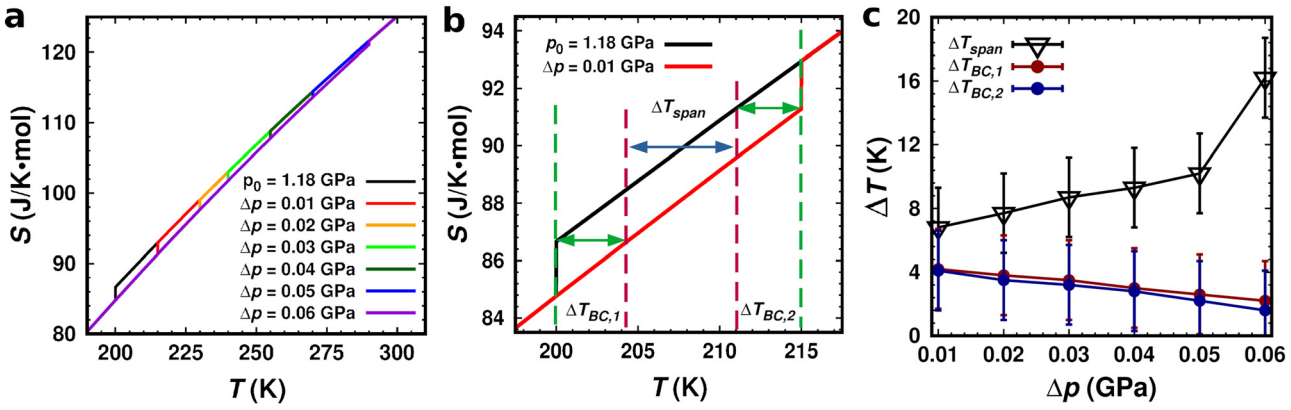

Fig. 3 Barocaloric performance of $BFCO_{0.5}$ directly estimated using DFT-based first-principles methods. (a) Entropy curves expressed as a function of temperature and applied pressure shift, $\Delta p \equiv p - p_0$. (b) Direct estimation of the adiabatic temperature change, ΔT_{BC}, and temperature span increment, ΔT_{span}. The latter quantity is calculated among consecutive pressure shifts of 0.01 GPa; hence, for a total pressure shift of $\Delta p = \sum_i \Delta p_i$, the corresponding temperature span is $T_{span} = \sum_i \Delta T_{span,i}$. (c) Barocaloric descriptors expressed as a function of the applied pressure shift.

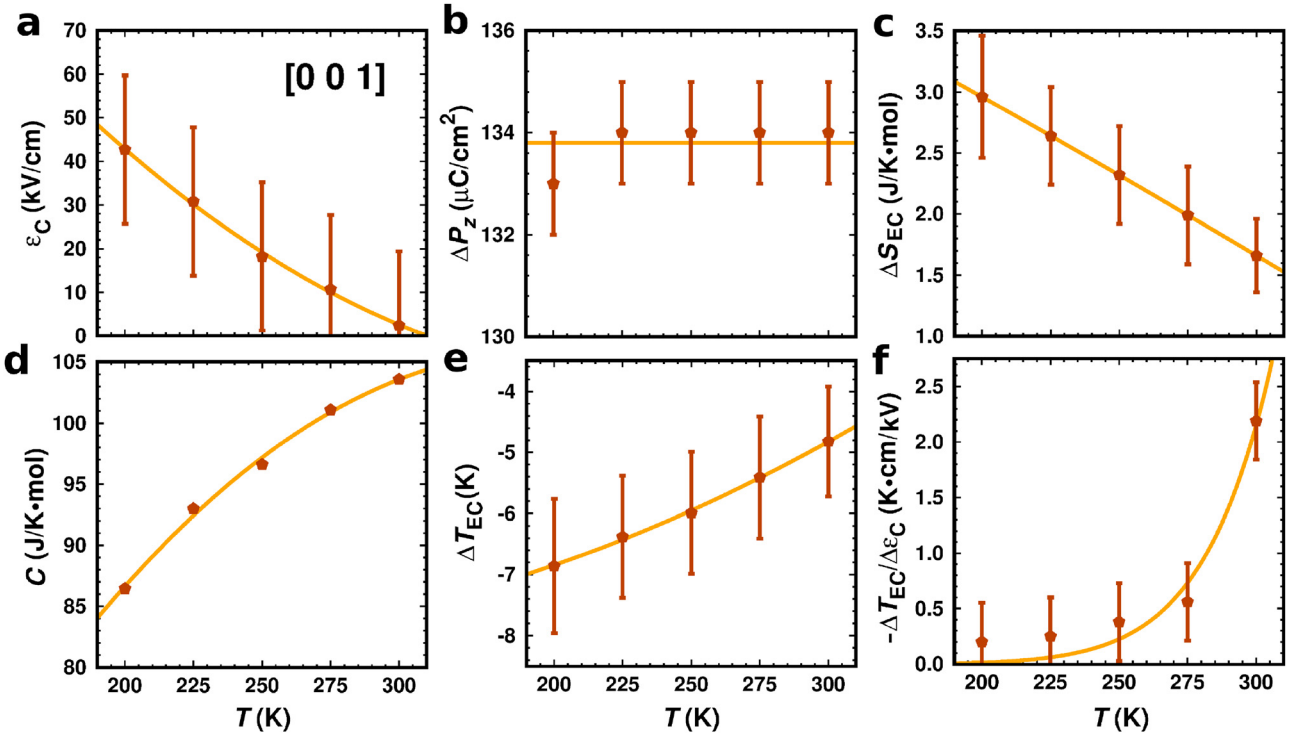

Fig. 4 Electrocaloric performance of $BFCO_{0.5}$ estimated using DFT-based first-principles methods at a fixed pressure of 1.25 GPa. (a) Critical electric field applied along the [001] direction inducing the $\mathcal{R} \rightarrow \mathcal{T}$ phase transition. (b) Electric polarization change along the [001] direction associated with the $\mathcal{E}$-induced $\mathcal{R} \rightarrow \mathcal{T}$ T phase transition. (c) Electrocaloric isothermal entropy change, ΔS_{EC}, calculated for the $\mathcal{E}$-induced $\mathcal{R} \rightarrow \mathcal{T}$ phase transformation in compressed $BFCO_{0.5}$. (d) Heat capacity of compressed $BFCO_{0.5}$. (e) Electrocaloric adiabatic temperature change, ΔT_{EC}, calculated for the $\mathcal{E}$-induced $\mathcal{R} \rightarrow \mathcal{T}$ phase transformation in compressed $BFCO_{0.5}$. (f) Electrocaloric strength of compressed $BFCO_{0.5}$. Both ΔS_{EC} and ΔT_{EC} were estimated by using the Clausius–Clapeyron relationship (Methods). Solid lines in the figure are simple eye-guides.

$|\Delta T_{BC}|$ since the underlying phase transitions are equivalent. For instance, at T = 200 K, we estimated an electrocaloric adiabatic temperature change of −6.9 K and at a room temperature of −4.8 K, to be compared with the analogous barocaloric shifts of +6.5 and +4.7 K. These ΔT_{EC} values are very much promising, specially when considering the small size of the required driving electric fields (that is, $\mathcal{E}_c \sim 1 - 10$ kV cm^{-1}).

Fig. 4f encloses results for the electrocaloric strength of $BFCO_{0.5}$, Λ_{EC}, expressed as a function of temperature; this quantity is defined as the ratio of ΔT_{EC} to the corresponding electric bias.[19] At T = 200 K, the attained adiabatic temperature change is highest; however, the required switching electric field is also largest, thus the resulting electrocaloric strength is smaller than the one obtained at higher temperatures. Still, the calculated Λ_{EC} amounting to 0.2 K cm kV^{-1} is already comparable to the record experimental values reported for oxide and hybrid organic–inorganic perovskites.[2,3,10] Remarkably, under increasing temperature, the electrocaloric strength of $BFCO_{0.5}$ noticeably increases reaching a maximum, and a colossal value of 2.2 K cm kV^{-1} at T = 300 K. These figures will be put into context in a next section; in what follows, we explain how the dual response of $BFCO_{0.5}$ to mechanical and electric stimuli may be exploited in practical solid-state cooling cycles.

Proposed $p - \mathcal{E}$ multicaloric cycle.

Single stimulus solid-state cooling cycles typically consist of four thermodynamic steps, two involving the adiabatic switching on and off of the applied external field and the other two constant-field heat transfer processes with the environment and the system to be refrigerated.[35] In the present work, we propose an original multi-stimuli solid-state cooling cycle consisting of eight thermodynamic steps that has been designed to minimize the applied electric field, thus maximizing Λ_{EC}, and with a cumulative multicaloric performance of $|\Delta T_{MC}| = |\Delta T_{BC}| + |\Delta T_{EC}|$ and $|\Delta S_{MC}| = |\Delta S_{BC}| + |\Delta S_{EC}|$.

Fig. 5 shows the envisaged multi-stimuli solid-state cooling cycle comprising hydrostatic pressure and electric fields being applied on multiferroic lead-free BFCO solid solutions near room temperature. The cycle starts with multiferroic BFCO in the supertetragonal $\mathcal{T}$ phase at temperature T. Subsequently, hydrostatic pressure is adiabatically applied on BFCO so that it transforms into the $\mathcal{R}$ phase and experiences a temperature increase of $|\Delta T_{BC}|$. In the third step, heat is released to the ambient, δQ_{BC}, and the initial temperature of the cycle is restored; compressed BFCO still remains in the $\mathcal{R}$ phase. Next, an electric field is adiabatically applied on compressed BFCO so that it transforms into the $\mathcal{T}$ phase, thus experiencing a temperature decrease of $|\Delta T_{EC}|$. In the fifth step, heat is absorbed by the system, δQ_{EC}, and the initial temperature of the cycle is restored; compressed and electrically biased BFCO remains in the $\mathcal{T}$ phase. Subsequently, the electric field is adiabatically removed thus BFCO transforms into the $\mathcal{R}$ phase and experiences a temperature increase of $|\Delta T_{EC}|$. In the seventh step, heat

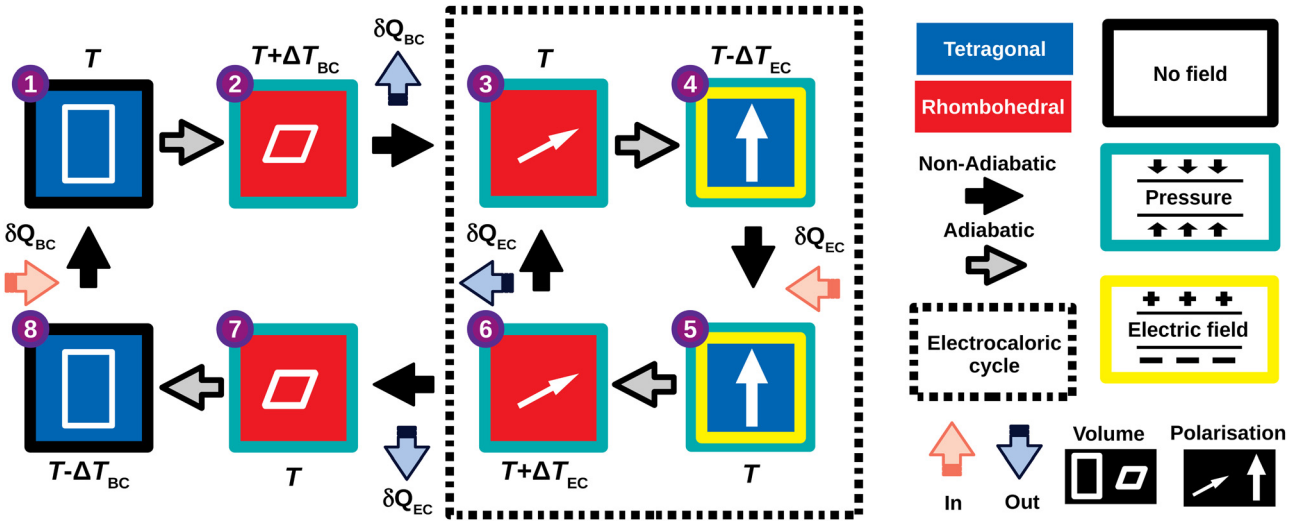

Fig. 5 Sketch of the proposed $p-\mathcal{E}$ multicaloric cycle for the enhancement of the electrocaloric strength. (1) The multiferroic compound BFCO is at equilibrium in the $\mathcal{T}$ phase at temperature T. (2) Hydrostatic pressure is adiabatically applied on BFCO so that it transforms into the $\mathcal{R}$ phase and experiences a temperature increase of $|\Delta T_{BC}|$. (3) Heat, δQ_{BC}, is released to the ambient and the initial temperature is restored; compressed BFCO remains in the $\mathcal{R}$ phase. (4) An electric field is adiabatically applied on compressed BFCO so that it transforms into the $\mathcal{T}$ phase and experiences a temperature decrease of $|\Delta T_{EC}|$. (5) Heat, δQ_{EC}, is absorbed by the system and the initial temperature is restored; compressed and electrically biased BFCO remains in the $\mathcal{T}$ phase. (6) The electric field is adiabatically removed from compressed BFCO, thus it transforms into the $\mathcal{R}$ phase and experiences a temperature increase of $|\Delta T_{EC}|$. (7) Heat, δQ_{EC}, is released to the ambient and the initial temperature is restored; compressed BFCO remains in the $\mathcal{R}$ phase. The state reached in this step is equivalent to that in step (3), thus one can repeatedly run the electrocaloric subcycle (3)–(6) entailing the application and removal of an electric bias under fixed hydrostatic pressure (dashed lines). (8) Hydrostatic pressure is adiabatically released from BFCO so that it transforms into the $\mathcal{T}$ phase and experiences a temperature decrease of $|\Delta T_{BC}|$. Heat, δQ_{BC}, is absorbed by the system and the starting temperature is restored, realizing an entire multicaloric (1)–(8) cycle.

is released to the ambient, δQ_{EC}, and the initial temperature of the cycle is restored; compressed BFCO remains in the $\mathcal{R}$ phase. Finally, hydrostatic pressure is adiabatically released so that BFCO transforms back into the $\mathcal{T}$ phase and experiences a temperature decrease of $|\Delta T_{BC}|$. Then, heat is absorbed by the system, δQ_{BC}, and the initial temperature of the cycle is restored, thus completing an entire multi-stimuli cycle.

Upon the completion of a multi-stimuli cycle, multiferroic BFCO is able to remove an amount of heat equal to $|\delta Q_{BC}| + |\delta Q_{EC}|$, or equivalently, $T\,(|\Delta S_{BC}| + |\Delta S_{EC}|)$, from the targeted system to be refrigerated and release it to the ambient (thus cooling it down). The described multi-stimuli cycle lends itself to several useful variations. For instance, the state reached in the seventh step is thermodynamically equivalent to that attained in the third step; therefore, one could recursively perform the electrocaloric subcycle consisting of steps (3)–(6) which entails the application and removal of an electric bias under fixed hydrostatic pressure (dashed lines in Fig. 5). Likewise, if the multi-stimuli cooling cycle started with multiferroic BFCO in the rhombohedral $\mathcal{R}$ phase instead of the $\mathcal{T}$ phase (*e.g.*, due to some compositional synthesis constraints), then the sequential application of hydrostatic pressure and electric fields explained above should be swapped.

Discussion

Table 1 summarizes some representative materials for which EC effects at or near room temperature have been experimentally

Table 1 Electrocaloric performance of several ferroelectric materials at or near room temperature. The theoretical electrocaloric strength, $\Lambda_{EC} \equiv |\Delta T_{EC}|/\mathcal{E}_c$, of compressed $BFCO_{0.5}$ is significantly larger than the experimental Λ_{EC} of other uncompressed ferroelectric compounds

	T (K)	$\mathcal{E}_c$ (kV cm^{-1})	ΔT_{EC} (K)	$\lvert\Delta T_{EC}\rvert/\mathcal{E}_c$ (K cm kV^{-1})	Ref.
Y-HfO_2	358	3500	24.8	0.01	5 (Expt.)
0.93PMN-0.07PT	298	723	9.0	0.01	37 (Expt.)
$(NH_4)_2SO_4$	220	400	4.5	0.01	42 (Expt.)
Terpolymer/PMN-PT	303	1800	31.0	0.02	38 (Expt.)
$Ba_{0.65}Sr_{0.35}TiO_3$	293	130	3.1	0.02	40 (Expt.)
$BaZr_{0.2}Ti_{0.8}O_3$	313	145	4.5	0.03	39 (Expt.)
BNBT-BCZT	370	620	23.0	0.04	9 (Expt.)
$PbZr_{0.46}Sn_{0.46}Ti_{0.08}O_3$	317	30	1.6	0.05	4 (Expt.)
$0.73Pb(Mg_{1/3}Nb_{2/3})O_3$–$0.27PbTiO_3$	300	10	2.5	0.25	41 (Expt.)
$BaTiO_3$	400	4.0	0.9	0.23	2 and 3 (Expt.)
$[(CH_3)_2CHCH_2NH_3]_2PbCl_4$	302	30	11.1	0.37	10 (Expt.)
$BFCO_{0.5}$ (pressurized)	300	2.2	−4.8	2.18	This work (Theory)

measured and reported in the literature. The selected compounds belong to three different families of ferroelectric materials, namely, oxides (*e.g.*, HfO_2 and $BaTiO_3$), hybrid organic–inorganic perovskites ($[(CH_3)_2CHCH_2NH_3]_2PbCl_4$) and polymers (terpolymer). In terms of largest $|\Delta T_{EC}|$, the oxides Y-HfO_2[5] and BNBT-BCZT[9] and the elastomer terpolymer/PMN-PT[38] emerge as the most promising materials since they display colossal values of 20–30 K. Nevertheless, these record materials require quite large electric fields to realize their full EC potential $(\mathcal{E}_c \sim 10^3\ \text{kV cm}^{-1})$, hence with no exception their associated electrocaloric strengths turn out to be quite mediocre, namely, $\Lambda_{EC} \sim 0.01\ \text{K cm kV}^{-1}$.

Ferroelectric materials exhibiting moderate or even small $|\Delta T_{EC}|$ but attained under smaller electric fields $(\mathcal{E}_c \sim 10\ \text{kV cm}^{-1})$, on the other hand, become the clear winners in terms of largest Λ_{EC}. For instance, the archetypal perovskite oxide $BaTiO_3$ renders an adiabatic temperature change of roughly 1 K driven by a minute electric field of 4 kV cm^{-1}, thus leading to a huge electrocaloric strength of 0.23 K cm kV^{-1}.[2,3] Likewise, $0.73Pb(Mg_{1/3}Nb_{2/3})O_3$–$0.27PbTiO_3$ renders a remarkable value of 0.25 K cm kV^{-1}[41] and the hybrid organic–inorganic perovskite $[(CH_3)_2CHCH_2NH_3]_2PbCl_4$ holds a record Λ_{EC} of 0.37 K cm kV^{-1}, which results from a small electric field of 30 kV cm^{-1} and an adiabatic temperature change of 11.1 K.[10] It is worth noting that all these figures correspond to experimental data.

Table 1 also encloses the EC results that we have theoretically estimated in this study for pressurized $BFCO_{0.5}$ at room temperature. According to our QHA-DFT calculations, compressed multiferroic BFCO solid solutions have the potential to surpass all previously known EC materials in terms of largest Λ_{EC}. In particular, we predict an outstanding electrocaloric strength of 2.18 K cm kV^{-1} that arises from an adiabatic temperature change of 4.8 K and an electric bias of $\approx$2 kV cm^{-1}. This theoretically estimated Λ_{EC} value is from one to two orders of magnitude larger than those experimentally measured in uncompressed ferroelectrics. The key mechanism in achieving such a colossal figure is to employ an ancillary field, in our case hydrostatic pressure, to bring the system towards the verge of a ferroelectric phase transition so that it is possible to drive it with a minuscule electric field.

In the specific case considered here, the pressure required to achieve a colossal Λ_{EC} value of 2.18 K cm kV^{-1} is higher than 1 GPa. Obviously, this compression is too large to be considered for practical applications. Nevertheless, as it was argued at the beginning of the Results section, it is possible to significantly reduce the size of this ancillary pressure to the order of several 0.1 GPa by decreasing the relative content of cobalt ions down to a critical composition of $\approx$0.25, without substantially affecting the main conclusions presented above. In particular, we calculated the vibrational properties of a multiferroic BFCO solid solution with a cobalt content of exactly 25%, $BFCO_{0.25}$, both in the $\mathcal{T}$ and $\mathcal{R}$ phases. At room temperature and under no pressure, the entropy difference between the two crystal structures was equal to 1.3 J K^{-1} mol^{-1} (disregarding thermal expansion effects), which matches within the numerical uncertainties the $|\Delta S_{BC}|$ of 1.7 $\pm$ 0.4 J K^{-1} mol^{-1} calculated for compressed $BFCO_{0.5}$ under the same thermodynamic conditions (Fig. 2c). Moreover, the relative volume change and electric polarization difference between the $\mathcal{T}$ and $\mathcal{R}$ phases respectively amount to $\approx$9% and $\approx$110 μC cm^{-2}, which in this case also turn out to be very much similar to the corresponding values estimated for $BFCO_{0.5}$ under equivalent thermodynamic conditions.

It is also worth noting that the Λ_{EC} enhancement approach proposed in this study, and theoretically demonstrated for $BFCO_{0.5}$, in principle should be generalizable to many other well-known EC materials since most of them are responsive to pressure as well (even though the magnitude of the resulting BC effects may be quite small in comparison to those achieved in state-of-the-art barocaloric materials). Take the archetypal ferroelectric compound $BaTiO_3$ as an example. The ferro- to paraelectric phase transition temperature in this material can be effectively shifted with pressure, namely, $dT_t/dp \approx -25\ \text{K GPa}^{-1}$;[43] thus, its room-temperature EC performance could be potentially improved with our proposed strategy.[12,16] Finally, to mention that recent developments in the synthesis of ferroelectric membranes and thin films may also allow for the enhancement of the Λ_{EC} figure-of-merit by combining electric fields with other types of mechanical stimuli like uniaxial[44] and biaxial[45] stress.

In conclusion, we have proposed a new strategy for the enhancement of the electrocaloric strength of ferroelectric materials that consists of concertedly applying pressure and electric fields. We have theoretically proved our new concept on multifunctional BFCO solid solutions, an intriguing family of compounds displaying a discontinuous phase transition between two multiferroic states. In particular, for compressed $BFCO_{0.5}$, we estimated a record Λ_{EC} parameter of 2.18 K cm kV^{-1} at room temperature resulting from an adiabatic temperature change of 4.8 K and an electric bias of $\approx$2 kV cm^{-1}. This electrocaloric strength turns out to be colossal since it is about one order of magnitude larger than those experimentally measured in uncompressed ferroelectrics ($\sim$0.1 K cm kV^{-1}). The demonstrated Λ_{EC} enhancement strategy can be applied to other types of ferroelectric materials, not necessarily magnetic, and be modified at convenience on the mechanical component. Thus, the combination of multiple stimuli opens new horizons in the field of caloric materials and solid-state refrigeration by expanding the design of possible cooling cycles and boosting caloric performance descriptors. We hope that the present theoretical study will motivate new experimental works on the engineering of original and environmentally friendly solid-state cooling devices.

Methods

Spin-polarized DFT calculations were performed with the generalized gradient approximation proposed by Perdew, Burke and Ernzerhof (PBE) as it is implemented in the VASP package.[46,47] The "Hubbard-*U*" scheme due to Dudarev *et al.* was employed in the PBE calculations for treating better the Co (Fe) 3d electrons, adopting a *U* value of 6 (4) eV.[22–25,48] The "projected augmented wave" method[49] was used to represent the ionic cores considering the following electronic states as valence: Co $4s^1 3d^8$, Fe $3p^6 4s^1 3d^7$,

Bi $6s^2 5d^{10} 6p^3$, and O $2s^2 2p^4$. An energy cut-off of 800 eV and a Γ-centered k-point grid of $4 \times 6 \times 6$ were employed for a $2 \times \sqrt{2} \times \sqrt{2}$ simulation cell containing 20 atoms,[50] thus obtaining zero-temperature energies converged to within 0.5 meV per formula unit. Geometry relaxations were performed for an atomic force threshold of 0.005 eV $Å^{-1}$. Electric polarizations were accurately estimated with the hybrid HSE06 functional[51] and the Berry phase formalism.[52–54]

Ab initio free energies were estimated within the quasi-harmonic approximation (QHA)[23,26,55] as a function of p and T. Phonon frequencies were calculated using the small displacement method.[55] The following technical parameters provided QHA free energies converged to within 5 meV per formula unit: 160-atom supercells, atomic displacements of 0.01 Å, and q-point grids of $16 \times 16 \times 16$ for integration within the first Brillouin zone. The effects of chemical disorder were addressed by generating all possible atomic Co–Fe and magnetic spin arrangements (ferromagnetic–FM– and antiferromagnetic–AFM–of type A, C, and G) for a $2 \times 2\sqrt{2} \times \sqrt{2}$ supercell containing 40 atoms. Quasi-harmonic free energies were calculated only for the lowest-energy configurations. Our spin-polarized DFT calculations were performed for bulk $BiFe_{0.5}Co_{0.5}O_3$.

Within the QHA,[23,26,55] the Gibbs free energy of a given crystal phase, G_{harm}, is expressed as follows:

$$G_{\text{harm}}(p, T) = E(p) + pV(p, T) + F_{\text{harm}}(p, T), \quad (1)$$

where E is the static energy of the system (*i.e.*, as directly obtained from zero-temperature DFT calculations), p is the pressure, V is the volume, and F_{harm} is the lattice Helmholtz free energy. (The dependence of different energy terms on p and T has been explicitly noted.) For given V and T, F_{harm} can be determined using the formula:

$$F_{\text{harm}}(V, T) = \frac{1}{N_q} k_B T \times \sum_{\mathbf{q}s} \ln\left[2 \sin h\left(\frac{\hbar\omega_{\mathbf{q}s}}{2k_B T}\right)\right], \quad (2)$$

where $\omega_{\mathbf{q}s}(V)$ are the phonon frequencies obtained at the reciprocal lattice vector $\mathbf{q}$ and phonon branch s, N_q is the total number of wave vectors used for integration in the Brillouin zone, and k_B is the Boltzmann constant. Meanwhile, the hydrostatic pressure p is calculated *via* the following expression:

$$p(V, T) = -\frac{\partial[E(V) + F_{\text{harm}}(V, T)]}{\partial V}, \quad (3)$$

which numerically allows $V(p, T)$ to be determined. Thus, by performing E and ω_{qs} DFT calculations for a set of V points, over which interpolation is applied to describe F_{harm} and p continuously, and by using eqn (1)–(3), it is possible to estimate $G_{\text{harm}}(p, T)$. To quantify the temperature at which the $\mathcal{T} \leftrightarrow \mathcal{R}$ phase transition occurs at a given pressure, T_t, the condition $\Delta G_{\text{harm}}(p, T_t) \equiv G^{\mathcal{T}}_{\text{harm}}(p, T_t) - G^{\mathcal{R}}_{\text{harm}}(p, T_t) = 0$ was employed.

Likewise, the entropy of the crystal can be obtained through the following expression:

$$S(V, T) = -\left(\frac{\partial F_{\text{harm}}}{\partial T}\right)_V, \quad (4)$$

and the heat capacity like:

$$C(V, T) = k_B \sum_{\mathbf{q}s} \left(\frac{\hbar\omega_{\mathbf{q}s}}{k_B T}\right)^2 \times \frac{\exp(\hbar\omega_{\mathbf{q}s}/k_B T)}{\left[\exp(\hbar\omega_{\mathbf{q}s}/k_B T) - 1\right]^2}. \quad (5)$$

Through the knowledge of $V(p, T)$ and eqn (2)–(5), then it is possible to determine $S(p, T)$ and $C(p, T)$.

In the absence of electric fields, the isothermal entropy change associated with barocaloric effects was approximately estimated using the Clausius–Clapeyron (CC) method like:[34]

$$\Delta S_{\text{BC}}(p, T) = \Delta V \cdot \frac{\mathrm{d}p_t}{\mathrm{d}T}, \quad (6)$$

where ΔV is the change in volume occurring during the phase transition and $p_t(T)$ is the critical pressure. Likewise, the corresponding adiabatic temperature change can be approximated using the expression:[56]

$$\Delta T_{\text{BC}}(p, T) = -\frac{T}{C} \cdot \Delta S_{\text{BC}}(p, T), \quad (7)$$

where $C(T)$ is the heat capacity of the system at zero pressure.

In the presence of electric fields, and assuming zero pressure, the thermodynamic potential that describes a particular phase is the Gibbs free energy defined as $G_{\text{harm}} = E - \boldsymbol{\mathcal{E}} \cdot \boldsymbol{P} + F_{\text{harm}}$, where E and F_{harm} are the same terms that appear in eqn (1), $\boldsymbol{P}$ is the electric polarization and $\boldsymbol{\mathcal{E}}$ is the applied electric field. In this case, the thermodynamic condition that determines the $\mathcal{E}$-induced phase transition is $G^{\mathcal{T}}_{\text{harm}}(T, \mathcal{E}_c) = G^{\mathcal{R}}_{\text{harm}}(T, \mathcal{E}_c)$. The value of the corresponding critical electric field then can be estimated as

$$\mathcal{E}_c(T) = \frac{\Delta(E + F_{\text{harm}}(T))}{\Delta P(T)}, \quad (8)$$

where $\Delta(E + F_{\text{harm}})$ is the Helmholtz free energy difference between the two phases, and ΔP is the resulting change in the electric polarization along the electric field direction. For $p \neq 0$ conditions, an additional $p\Delta V$ term should be considered in the right-hand side of eqn (8).

Once the value of $\mathcal{E}_c$ and its dependence on temperature are determined through eqn (8), the isothermal entropy change associated with electrocaloric effects can be approximately estimated using the CC method as[25]

$$\Delta S_{\text{EC}}(E, T) = -\Delta P \cdot \frac{\mathrm{d}\mathcal{E}_c}{\mathrm{d}T}. \quad (9)$$

Likewise, the corresponding adiabatic temperature change was approximated using the expression:[56]

$$\Delta T_{\text{EC}}(\mathcal{E}, T) = -\frac{T}{C} \cdot \Delta S_{\text{EC}}(\mathcal{E}, T), \quad (10)$$

where $C(T)$ is the heat capacity of the system at zero electric field.

Conflicts of interest

There are no conflicts to declare.

Acknowledgements

We acknowledge financial support by the MCIN/AEI/10.13039/501100011033 under grants PID2020-119777GB-I00 and TED2021-130265B-C22, the "Ramón y Cajal" fellowship RYC2018-024947-I and the Severo Ochoa Centres of Excellence Program (CEX2019-000917-S), and by the Generalitat de Catalunya under grant no. 2017 SGR 1506. Computational support was provided by the Red Española de Supercomputación (RES) under the grants FI-2022-1-0012, FI-2022-1-0006, FI-2022-2-0003 and FI-2022-3-0014.

References

1 Y. Liu, J. F. Scott and B. Dkhil, Direct and indirect measurements on electrocaloric effect: Recent developments and perspectives, *Appl. Phys. Rev.*, 2016, **3**, 031102.
2 E. Stern-Taulats, P. Lloveras, M. Barrio, E. Defay, M. Egilmez, A. Planes, J.-L. Tamarit, L. Mañosa, N. D. Mathur and X. Moya, Inverse barocaloric effects in ferroelectric $BaTiO_3$ ceramics, *APL Mater.*, 2016, **4**, 091102.
3 X. Moya, E. Stern-Taulats, S. Crossley, D. González-Alonso, S. Kar-Narayan, A. Planes, L. Mañosa and N. D. Mathur, Giant electrocaloric strength in single-crystal $BaTiO_3$, *Adv. Mater.*, 2013, **25**, 1360.
4 P. D. Thacher, Electrocaloric effects in some ferroelectric and antiferroelectric $Pb(Zr,Ti)O_3$ compounds, *J. Appl. Phys.*, 1968, **39**, 1996.
5 S. Samanta, G. Anoop, W. Seol, S. M. Park, H. Joh, J. O. Choi, D. Ahn, S. Unithrattil, H. Kim, J. Yeom, S. Hong and J. Y. Jo, Large electrocaloric effect with high thermal and electric field cycling stability in solution-processed $Y:HfO_2$ thin films, *J. Mater. Chem. A*, 2022, **10**, 9960.
6 A. S. Mischenko, Q. Zhang, J. F. Scott, R. W. Whatmore and N. D. Mathur, Giant electrocaloric effect in thin-film $PbZr_{0.95}Ti_{0.05}O_3$, *Science*, 2006, **311**, 1270.
7 B. Neese, B. Chu, S.-G. Lu, Y. Wang, E. Furman and Q. Zhang, Large electrocaloric effect in ferroelectric polymers near room temperature, *Science*, 2008, **321**, 821.
8 B. Asbani, Y. Gagou, J.-L. Dellis, M. Trcek, Z. Kutnjak, M. Amjoud, A. Lahmar, D. Mezzane and M. El Marssi, Lead-free $Ba_{0.8}Ca_{0.2}Te_xTi_{1-x}O_3$ ferroelectric ceramics exhibiting high electrocaloric properties, *J. Appl. Phys.*, 2017, **121**, 064103.
9 S. E. Shirsath, C. Cazorla, T. Lu, L. Zhang, Y. Y. Tay, X. Lou, Y. Liu, S. Li and D. Wang, Interface-charge induced giant electrocaloric effect in lead free ferroelectric thin-film bilayers, *Nano Lett.*, 2020, **20**, 1262.
10 X. Liu, Z. Wu, T. Guan, H. Jiang, P. Long, X. Li, C. Ji, S. Chen, A. Sun and J. Luo, Giant room temperature electrocaloric effect in a layered hybrid perovskite ferroelectric: $[(CH_3)_2CHCH_2NH_3]_2PbCl_4$, *Nat. Commun.*, 2021, **12**, 5502.
11 R. E. Cohen, Origin of ferroelectricity in perovskite oxides, *Nature*, 1992, **358**, 136.
12 Y. Liu, J. Wei, P.-E. Janolin, I. C. Infante, X. Lou and B. Dkhil, Giant room-temperature barocaloric effect and pressure-mediated electrocaloric effect in $BaTiO_3$ single crystal, *Appl. Phys. Lett.*, 2014, **104**, 162904.
13 S. Patel, A. Chauhan, R. Vaish and C. S. Lynch, Large barocaloric effect and pressure-mediated electrocaloric effect in $Pb_{0.99}Nb_{0.02}$ $(Zr_{0.95}Ti_{0.05})_{0.08}O_3$ ceramics, *J. Am. Ceram. Soc.*, 2017, **100**, 4902.
14 A. Chauhan, S. Patel, S. Wang, N. Novak, B.-X. Xu, P. Lv, R. Vaish and C. S. Lynch, Enhanced performance of ferroelectric materials under hydrostatic pressure, *J. Appl. Phys.*, 2017, **122**, 224105.
15 Y.-K. Wang, Q.-L. Zhao, J. J. Di, G.-P. He, L. Zhao, T.-T. Su, M.-Y. Zhang, J. Zhang, X. Liang and D. Bu, Thermodynamic analysis of stress-mediated barocaloric effect, electrocaloric effect, and energy storage of $PbZrO_3$ antiferroelectric film, *Phys. Status Solidi A*, 2021, **218**, 2000651.
16 Y. Liu, G. Zhang, Q. Li, L. Bellaiche, J. F. Scott, B. Dkhil and Q. Wang, Towards multicaloric effect with ferroelectrics, *Phys. Rev. B: Condens. Matter Mater. Phys.*, 2016, **94**, 214113.
17 S. Lisenkov, B. K. Mani, C.-M. Chang, J. Almand and I. Ponomareva, Multicaloric effect in ferroelectric $PbTiO_3$ from first principles, *Phys. Rev. B: Condens. Matter Mater. Phys.*, 2013, **87**, 224101.
18 L. Liang, Y. L. Li, L.-Q. Chen, S. Y. Hu and G.-H. Lu, Thermodynamics and ferroelectric properties of $KNbO_3$, *J. Appl. Phys.*, 2009, **106**, 104118.
19 S.-G. Lu, X. Lin, J. Li, D. Li, Y. Yao, T. Tao and B. Liang, Enhanced electrocaloric strengths at room temperature in $(Sr_xBa_{1-x})(Sn_{0.05}Ti_{0.95})O_3$ lead-free ceramics, *J. Alloys Compd.*, 2021, **871**, 159519.
20 M. Azuma, S. Niitaka, N. Hayashi, K. Oka, M. Takano, H. Funakubo and Y. Shimakawa, Rhombohedral-tetragonal phase boundary with high Curie temperature in $(1-x)BiCoO_3$–$xBiFeO_3$ solid solution, *Jpn. J. Appl. Phys.*, 2008, **47**, 7579.
21 H. Hojo, K. Oka, K. Shimizu, H. Yamamoto, R. Kawabe and M. Azuma, Development of bismuth ferrite as a piezoelectric and multiferroic material by cobalt substitution, *Adv. Mater.*, 2018, **30**, 1705665.
22 C. Menéndez and C. Cazorla, Giant thermal enhancement of the electric polarization in ferrimagnetic $BiFe_{1-x}Co_xO_3$ solid solutions near room temperature, *Phys. Rev. Lett.*, 2020, **125**, 117601.
23 C. Cazorla and J. Íñiguez, Insights into the phase diagram of bismuth ferrite from quasiharmonic free-energy calculations, *Phys. Rev. B: Condens. Matter Mater. Phys.*, 2013, **88**, 214430.
24 C. Cazorla, O. Diéguez and J. Íñiguez, Multiple structural transitions driven by spin-phonon couplings in a perovskite oxide, *Sci. Adv.*, 2017, **3**, e1700288.
25 C. Cazorla and J. Íñiguez, Giant direct and inverse electrocaloric effects in multiferroic thin films, *Phys. Rev. B: Condens. Matter Mater. Phys.*, 2018, **98**, 174105.
26 C. Cazorla and J. Boronat, Simulation and understanding of atomic and molecular quantum crystals, *Rev. Mod. Phys.*, 2017, **89**, 035003.
27 A. Aznar, P. Lloveras and M. Romanini, *et al.*, Giant barocaloric effects over a wide temperature range in superionic conductor AgI, *Nat. Commun.*, 2017, **8**, 1851.
28 C. Cazorla and D. Errandonea, Giant mechanocaloric effects in fluorite-structured superionic materials, *Nano Lett.*, 2016, **16**, 3124.

29 A. K. Sagotra, D. Errandonea and C. Cazorla, Mechanocaloric effects in superionic thin films from atomistic simulations, *Nat. Commun.*, 2017, **8**, 963.
30 A. K. Sagotra, D. Chu and C. Cazorla, Room-temperature mechanocaloric effects in lithium-based superionic materials, *Nat. Commun.*, 2018, **9**, 3337.
31 P. Lloveras, A. Aznar and M. Barrio, *et al.*, Colossal barocaloric effects near room temperature in plastic crystals of neopentylglycol, *Nat. Commun.*, 2019, **10**, 1803.
32 B. Li, Y. Kawakita and S. Ohira-Kawamura, *et al.*, Colossal barocaloric effects in plastic crystals, *Nature*, 2019, **567**, 506.
33 C. Cazorla, Refrigeration based on plastic crystals, *Nature*, 2019, **567**, 470.
34 K. Sau, T. Ikeshoji, S. Takagi, S.-I. Orimo, D. Errandonea, D. Chu and C. Cazorla, Colossal barocaloric efects in the complex hydride $Li_2B_{12}H_{12}$, *Sci. Rep.*, 2021, **11**, 11915.
35 C. Cazorla, Novel mechanocaloric materials for solid-state cooling applications, *Appl. Phys. Rev.*, 2019, **6**, 041316.
36 J. Li, D. Dunstan, S. Lou, A. Planes, L. Mañosa, M. Barrio, J.-L. Tamarit and P. Lloveras, Reversible barocaloric effects over a large temperature span in fullerite C_{60}, *J. Mater. Chem. A*, 2020, **8**, 20354.
37 T. M. Correia, J. S. Young, R. W. Whatmore, J. F. Scott, N. D. Mathur and Q. Zhang, Investigation of the electrocaloric effect in a $PbMg_{1/3}Nb_{2/3}O_3$–$PbTiO_3$ relaxor thin film, *Appl. Phys. Lett.*, 2009, **95**, 182904.
38 C. Huang, H.-B. Yang and C.-F. Gao, Giant electrocaloric effect in cracked ferroelectrics, *J. Appl. Phys.*, 2018, **123**, 154102.
39 X.-S. Qian, H. J. Ye, Y. Zhang, H. Gu, X. Li, C. A. Randall and Q. M. Zhang, Giant electrocaloric response over a broad temperature range in modified $BaTiO_3$ ceramics, *Adv. Funct. Mater.*, 2014, **24**, 1300.
40 X. Q. Liu, T. T. Chen, Y. J. Wu and X. M. Chen, Enhanced electrocaloric effects in spark plasma-sintered $Ba_{0.65}Sr_{0.35}TiO_3$ -based ceramics at room temperature, *J. Am. Ceram. Soc.*, 2013, **96**, 1021.
41 B. Lu, X. Jian, X. Lin, Y. Yao, T. Tao, B. Liang, H. Luo and S.-G. Lu, Enhanced electrocaloric effect in 0.73Pb$(Mgi_{1/3}Nb_{2/3})O_3$ -0.27$PbTiO_3$ single crystals via direct measurement, *Crystals*, 2020, **10**, 451.
42 S. Crossley, W. Li, X. Moya and N. D. Mathur, Large electrocaloric effects in single-crystal ammonium sulfate, *Philos. Trans. R. Soc., A*, 2016, **374**, 20150313.
43 S. A. Hayward and E. K. H. Salje, The pressure-temperature phase diagram of $BaTiO_3$: a macroscopic description of the low-temperature behaviour, *J. Phys.: Condens. Matter*, 2002, **14**, L599.
44 Y. Zang, C. Di and Z. Geng, *et al.*, Giant thermal transport tuning at a metal/ferroelectric interface, *Adv. Mater.*, 2022, **34**, 2105778.
45 Y. Liu, L. C. Phillips, R. Mattana, M. Bibes, A. Barthélémy and B. Dkhil, Large reversible caloric effect in FeRh thin films via a dual-stimulus multicaloric cycle, *Nat. Commun.*, 2016, **7**, 11614.
46 G. Kresse and J. Furthmüller, Efficient iterative schemes for ab initio total-energy calculations using a plane-wave basis set, *Phys. Rev. B: Condens. Matter Mater. Phys.*, 1996, **54**, 11169.
47 J. P. Perdew, K. Burke and M. Ernzerhof, Generalized gradient approximation made simple, *Phys. Rev. Lett.*, 1996, **77**, 3865.
48 C. Menéndez, D. Chu and C. Cazorla, Oxygen-vacancy induced magnetic phase transitions in multiferroic thin films, *npj Comput. Mater.*, 2020, **6**, 76.
49 P. E. Blöchl, Projector augmented-wave method, *Phys. Rev. B: Condens. Matter Mater. Phys.*, 1994, **50**, 17953.
50 C. Cazorla and M. Stengel, Electrostatic engineering of strained ferroelectric perovskites from first principles, *Phys. Rev. B: Condens. Matter Mater. Phys.*, 2015, **92**, 214108.
51 J. Heyd, G. E. Scuseria and M. Ernzerhof, Hybrid functionals based on a screened Coulomb potential, *J. Chem. Phys.*, 2003, **118**, 8207.
52 R. D. King-Smith and D. Vanderbilt, Theory of polarization of crystalline solids, *Phys. Rev. B: Condens. Matter Mater. Phys.*, 1993, **47**, 1651.
53 R. Resta, Macroscopic polarization in crystalline dielectrics: the geometric phase approach, *Rev. Mod. Phys.*, 1994, **66**, 899.
54 L. Bellaiche and D. Vanderbilt, Intrinsic piezoelectric response in perovskite alloys: PMN-PT versus PZT, *Phys. Rev. Lett.*, 1999, **83**, 1347.
55 A. Togo and I. Tanaka, First principles phonon calculations in materials science, *Scr. Mater.*, 2015, **108**, 1.
56 L. Mañosa and A. Planes, Materials with giant mechanocaloric effects: Cooling by strength, *Adv. Mater.*, 2017, **29**, 1603607.